

Triblock Copolymer Pluronic F68 as a Corrosion Inhibitor for Aluminum-air Battery: An Electrochemical and in Silico Study

Lei Guo^{1,*}, Jianhong Tan², Hong Yang¹, Youness El Bakri^{3,4}, Savaş Kaya⁵, Senlin Leng¹, Yingchang Yang¹, Wei Shi¹

¹ School of Material and Chemical Engineering, Tongren University, Tongren 554300, China

² School of Chemistry and Chemical Engineering, Yangtze Normal University, Chongqing 408100, China

³ Laboratoire de Chimie Organique Hétérocyclique, Centre de Recherche des Sciences des Médicaments, Pôle de Compétences Pharmacochimie, URAC 21, Faculté des Sciences, Mohammed V University Rabat, Avenue Ibn Battouta, BP 1014, Rabat, Morocco

⁴ Department of Organic Chemistry, Science Faculty, RUDN University Miklukho-Maklayast.6, Moscow 117198, Russian Federation

⁵ Department of Chemistry, Faculty of Science, Cumhuriyet University, Sivas 58140, Turkey

*E-mail: cqglei@163.com

Received: 9 July 2019 / Accepted: 6 September 2019 / Published: 29 October 2019

In Al-air batteries, the self-corrosion of aluminum electrodes is an issue worthy of concern. In this paper, the inhibition performance and anti-corrosion mechanism of a triblock copolymer, namely, Pluronic F68, on Al in 3.5% NaCl electrolyte are investigated with a multidimension approach combining electrochemical and theoretical approaches. The results suggest that Pluronic F68 inhibitor can present wonderful anticorrosion efficiency, and the maximum inhibition efficiency can reach 94% at low dose concentration. Meanwhile, the battery containing Pluronic F68 exhibits better performance. Significantly, the present work is beneficial to understand the inhibition mechanism of similar organic polymers and provides a feasible approach to develop Al-air batteries.

Keywords: Al-air battery, Corrosion inhibition, Electrochemistry; Theoretical calculations

1. INTRODUCTION

Nowadays, the problem of energy crisis is becoming more and more serious than ever before. Lithium-ion batteries have been far from enough to satisfy the urgent demands for portable devices, electrical vehicles, etc. Fortunately, metal-air batteries have being rapidly developed as supplemental energy, which combine a metallic negative electrode with an air electrode [1-3]. Among them, Al-air

batteries are the best power candidates on account of their high theoretical energy density (8100 Wh g^{-1}), environmental friendliness, and low consumption. The basic structure for a normal Al-air battery is schematically illustrated in Figure 1, which is composed of an Al anode, electrolyte as well as breathable air cathode. The electrolytes are generally neutral or alkaline media, such as NaCl, KOH, or NaOH solutions. It affords electrical energy through electron transfer reactions between anode and the cathode. The reactions can be expressed as follows when the electrolyte is neutral [4, 5]:

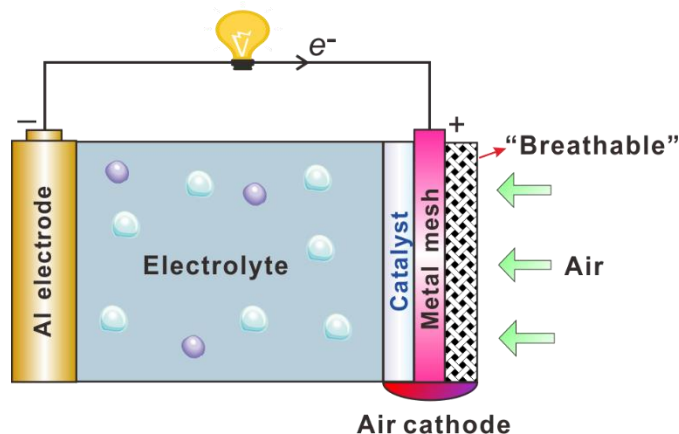


Figure 1. Illustration of the structure of an Al-air battery using a 3-layer air electrode.

According to investigation statistics, many scientists concentrated on the study of cathode catalyst, we have to admit that this is an effective strategy to improve the performance of Al-air batteries [6-8]. But on the other hand, we should also pay attention to the self-corrosion of Al anode, which results in a reduction of anode utilization [9, 10]. Generally, the Al electrode is vulnerable to chloride ions in neutral electrolyte, wherein the compact oxide film on Al surface can be attacked and damaged. There are two common methods to solve this problem. The first one is alloying Al with other minor elements such as Ga, In, Sn, Mn [11-14], but this method increases the material cost. The second method is the use of additives to the electrolyte for inhibiting the anode corrosion. Deyab have reported that nonionic surfactant [15], ionic liquid [16] can be served as effective corrosion inhibitors for Al-air battery. It is generally recognized that the inhibitor molecules act by adsorbing on the metal surface, which can lead to the decrease of corrosion rate [17, 18].

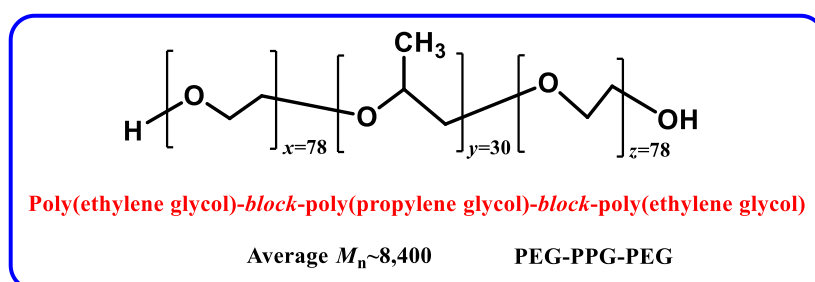


Figure 2. The molecular structure of pluronic F68.

In this account, a triblock copolymer, namely, Pluronic F68 or PEG-PPG-PEG (see Figure 2), was used as a potential inhibitor for Al electrode corrosion in Al-air battery. As is reported, PEG-PPG-PEG is usually used in cell culture as a stabilizer to protect the cell membranes against shear stress and additionally acts as an anti-foaming agent. It is a highly safe compound and can be biodegradable. The effectiveness and function mechanism of PEG-PPG-PEG as a corrosion inhibitor were evaluated using electrochemical and theoretical calculation methods. In addition, the performance of Al-air battery in the presence of PEG-PPG-PEG additive was also investigated.

2. EXPERIMENTAL DETAILS

2.1. Material and chemicals

Pure Al sheet (99.99%) was cut mechanically into 2.5 cm × 2.0 cm × 0.30 cm specimens and used as working electrodes. It was supplied by Shenzhen Jinrui Aluminium Industry Co., Ltd. (China). The total square area of the Al electrodes exposed to the electrolyte solution was 1 cm². Prior to electrochemical test, the Al specimen surface was mechanically abraded with SiC abrasive papers of different grades (400, 600, 800, 1000 and 1200), followed by washing with distilled water, degreasing in ethanol and cleaning with distilled water. PEG-PPG-PEG was purchased from Sigma-Aldrich. The range for the concentrations of PEG-PPG-PEG inhibitor concerned in this study was 0.3, 0.5, 1.0, 3.0 to 5.0 mM. The electrolyte solution 3.5% NaCl was prepared by dilution of AR grade 99% NaCl with distilled water.

2.2. Electrochemical experiments

The electrochemical measurements were carried out using conventional three-electrode system working on RST5000 electrochemical station. The Al electrode was put together with a platinum foil as a counter electrode and a saturated calomel electrode (SCE) as a reference electrode. The Al electrode was immersed in the corrosive solution for appropriate time until a steady-state potential was achieved. Subsequently, EIS measurements were performed by applying to the cell a 10 mV sine wave with frequencies in the range of 100 kHz to 0.01 Hz. The resultant data were analyzed using ZsimpWin 3.21 software. Finally, Tafel polarization curves were performed immediately after EIS measurements with scanning rate of 0.2 mV s⁻¹ commencing from -250 to +250 mV versus open-circuit-potential. The temperature of all those test solutions was maintained at 298 K by using a thermostatic water bath. In order to get good accuracy, all the measurements were conducted in triplicate.

2.3. Battery test

When it is discharging, the Al-air battery converts chemical energy to electrical energy. In this work, the discharge behavior of Al-air battery employing 3.5% NaCl electrolyte with and without PEG-PPG-PEG was carried out to assess the battery performance. Our Al-air battery was assembled with a

consumed Al anode, NaCl electrolyte, and a homemade cathode. Cathode was an air electrode consisting of a gas diffusion layer and a catalytic active layer, which were laminated with a nickel mesh as a current collector. The galvanostatic discharge test was conducted at a constant current density of 5.0 mA cm^{-2} for 5 h.

2.4. Theoretical calculations

In order to choose the appropriate adsorption surface, a prediction of Al crystal morphology was necessary before the simulation calculations. Herein, Bravais–Friedel–Donnay–Harker (BFDH) method was utilized to predict the crystal structures. More detailed descriptions about this model can be found elsewhere [19, 20]. The molecular dynamics (MD) simulations of inhibitor-Al interactions were assayed using the Materials Studio Forcite module. Water molecules had been considered in order to reveal the aqueous phase environment. MD simulation was implemented at 298.0 K under NVT canonical ensemble using a time step of 1.0 fs and simulation time of 1.0 ns by the COMPASSII forced field [21]. Non-bond interactions, van der Waals and electrostatic, were set as Atom-based and Ewald summation method, respectively, with a cutoff radius of 1.2 nm. The dynamic process was carried until both temperature and energy of the entire system were balanced.

3. RESULTS AND DISCUSSION

3.1. Electrochemical impedance spectra (EIS)

As a nondestructive electrochemical technique, EIS can quickly provide useful reaction information occurring on the metal surface. Thus, the effect of PEG-PPG-PEG additive at various concentrations on Al corrosion in NaCl solution was evaluated by EIS test and the results are given in the Nyquist diagrams, as shown in Figure 3a. We can find that the shapes of uninhibited and inhibited curves are very similar, revealing that the presence of PEG-PPG-PEG increases the impedance but does not change the other aspects of the electrode behaviour. The diameters of Nyquist plots increase with the increasing of inhibitor concentration. The obtained impedance spectra all contain a depressed semicircle with center below the real axis, which is a characteristic for metal electrodes. This phenomenon is known as the frequency dispersion and can be attributed to the roughness and inhomogeneities of the metal surface [22, 23].

To further investigate the actual properties of our corrosion system, Randles equivalent circuit (described in Figure 3b) was introduced to fit EIS data and the results were listed in Table 1. Low chisquared values indicated good fits. In Figure 3b, R_s is the solution resistance, R_f signifies the film resistance, R_{ct} is the charge transfer resistance, R_p is the polarization resistance between Al surface and outer Helmholtz plane, which is defined as $R_p = R_f + R_{ct}$. A constant phase element (CPE), as a substitute for the capacitor, is utilized to compensate for the inhomogeneity of electrodes. CPE_{dl} and CPE_f represent film capacitance and double layer capacitance, respectively [24]. The relevant impedance (Z_{CPE}) can be calculated by the following formula [25, 26]:

$$Z_{CPE} = \frac{1}{Y_0(j\omega)^n} \tag{4}$$

where Y_0 is the magnitude of the CPE, ω is the angular frequency, $j^2=-1$ is the imaginary number, and n is the CPE exponent. If $n=0$, CPE represents a pure resistor, for $n = -1$ an inductor, and for $n=1$, a pure capacitor [27]. The inhibited efficiency of PEG-PPG-PEG is calculated from the polarization resistance according to the following equation:

$$IE = \frac{R_p - R_{p,0}}{R_p} \times 100 \tag{5}$$

where $R_{p,0}$ and R_p are the polarization resistances for Al electrodes in 3.5% NaCl solution without and with PEG-PPG-PEG, respectively.

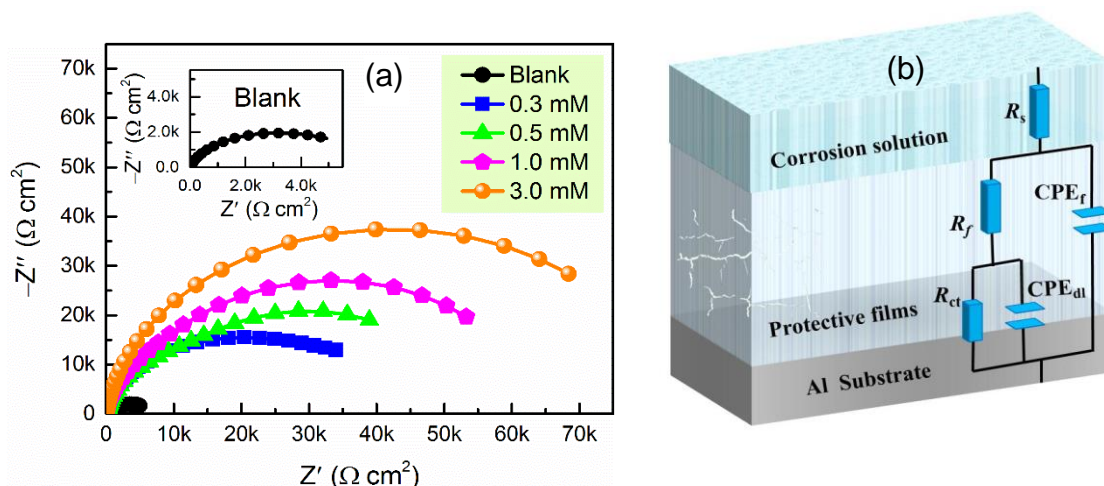


Figure 3. (a) Nyquist plot for the Al electrode with and without different concentrations of PEG-PPG-PEG; (b) Equivalent circuit used to fit the EIS loop.

As can be seen from Table 1, the R_p values increase significantly from 5.0 to 88.9 $k\Omega \cdot cm^2$ as the concentration of PEG-PPG-PEG increases. The maximum inhibition efficiency could reach 94.3% when the inhibitor concentration is 3 mM. This behavior can be attributed to the self-assembled barrier layer of polymer molecules by adsorbing on the Al surface, which ultimately results in the increment of R_p and the enhancement of inhibition efficiency. However, the adsorption of PEG-PPG-PEG molecules at the Al/solution interface can cause a decrease in local dielectric constant and/or an increase in the thickness of the double layer, thus resulting in the decrease of CPEs [28, 29].

Table 1. Impedance parameters for Al in 3.5% NaCl solution at 298 K without and with various concentrations of PEG-PPG-PEG.

C (mM)	R_s (Ωcm^2)	R_f ($k\Omega cm^2$)	CPE _f		CPE _{dl}		R_{ct} ($k\Omega cm^2$)	R_p ($k\Omega cm^2$)	ChiSq ($\times 10^{-3}$)	IE %
			$Y_0 (\times 10^{-5} S s^n cm^{-2})$	n_1	$Y_0 (\times 10^{-6} S s^n cm^{-2})$	n_2				
Blank	19.2	1.6	4.832	0.864	2.299	0.771	3.4	5.0	1.495	/
0.3	19.1	6.8	4.038	0.873	2.034	0.781	17.9	24.7	1.387	79.7
0.5	34.7	12.8	3.945	0.845	1.839	0.764	27.3	40.1	1.109	87.5
1.0	23.7	22.3	3.868	0.890	1.776	0.745	32.2	54.5	1.250	90.8
3.0	15.1	38.4	3.765	0.812	1.543	0.787	50.5	88.9	1.820	94.3

3.2. Polarization measurements

Tafel polarization curves for Al in 3.5% NaCl solution for different concentrations of PEG-PPG-PEG are depicted in Figure 4. The evaluated electrochemical parameters corrosion potential (E_{corr}), corrosion currents density (I_{corr}), anodic Tafel slopes (β_a), cathodic Tafel slopes (β_c), and inhibition efficiency (IE) values are listed in Table 2. Inhibition efficiency was defined as follows:

$$IE = \frac{I_{\text{corr},0} - I_{\text{corr}}}{I_{\text{corr},0}} \times 100 \quad (6)$$

where I_{corr} and $I_{\text{corr},0}$ represent the corrosion current densities in the presence or absence of inhibitors, respectively. Corrosion current densities were obtained by the extrapolation of the current–potential lines to the corresponding corrosion potentials.

As shown in Figure 4 and Table 2, the E_{corr} values of Al exhibited slightly change. The displacement in E_{corr} is less than 85 mV with respect to the blank, which indicates that PEG-PPG-PEG is a mixed-type inhibitor [30, 31]. In other words, the addition of PEG-PPG-PEG to 3.5% NaCl solution reduced the anodic dissolution of aluminum and retarded cathodic oxygen reduction [32], which led to a decrease in both the cathodic and anodic current density. In the presence of PEG-PPG-PEG, the slight change of both β_a and β_c suggests that the corrosion mechanism of Al does not change. The inhibitors reduce the corrosion of Al by blocking the active sites of the substrate. Besides, the inhibition efficiencies obtained from potentiodynamic polarization curves and EIS are in good reasonably agreement.

Table 2 Tafel parameters and the corresponding corrosion inhibition efficiency for the corrosion of Al in 3.5% NaCl solution in the absence and presence of different concentrations of PEG-PPG-PEG.

C (mM)	E_{corr} (mV/SCE)	I_{corr} ($\times 10^{-4}$ A cm^{-2})	β_a (mV dec^{-1})	$-\beta_c$ (mV dec^{-1})	IE %
Blank	-750	383	18	180	/
0.3	-763	100	22	161	73.8
0.5	-756	63.2	18	189	83.4
1.0	-761	39.8	24	167	89.6
3.0	-753	19.9	19	189	94.8

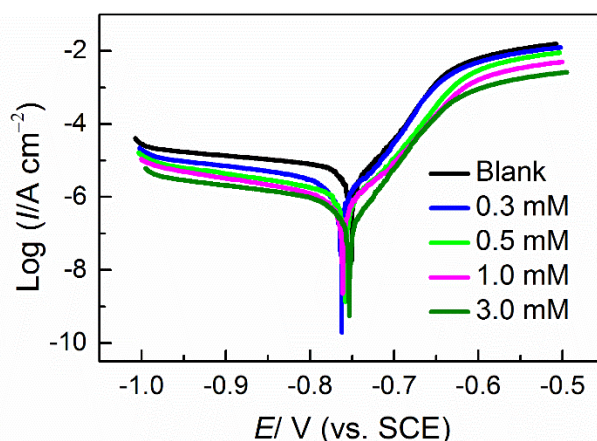


Figure 4. Potentiodynamic polarization curves of Aluminum in 3.5% NaCl solution in the absence and presence of different concentrations of PEG-PPG-PEG.

3.3. Al-air battery performance test

Aluminum-air cell discharge performances under selected current density in ambient temperature were investigated. Figure 5a displays the discharge behavior of the Al-air battery with and without 3 mM PEG-PPG-PEG at the current density of 5 mA cm^{-2} . As can be seen from Figure 5a, the average discharge voltage of the cell increased from 0.31 V to 0.35 V by adding PEG-PPG-PEG. This demonstrates that the addition of PEG-PPG-PEG in neutral electrolyte solution significantly improves the battery performance. This phenomenon can be ascribed to the low corrosion rate of Al electrode resulted from adsorption of inhibitor molecule on the Al electrode surface. To demonstrate the work ability via simple visual information, our assembled Al-air battery was used for powering a digital watch (Figure 5b). The long time operation indicated the strongly power output ability of Al-air batteries. We firmly believe that these batteries can be applied to electric vehicles or emergency standby power after multiple assembly.

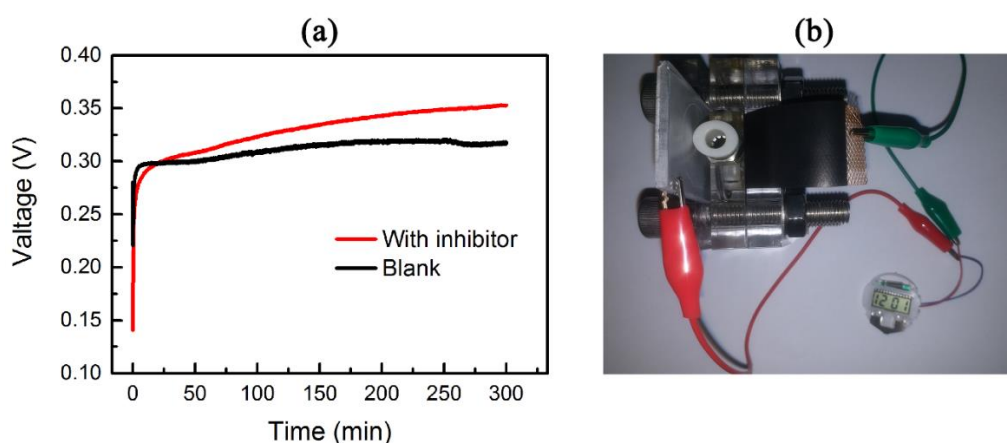


Figure 5. (a) Discharge behavior of Al-air battery at 5 mA cm^{-2} in the absence and presence of 3 mM of PEG-PPG-PEG; (b) The photograph of a digital watch powered by the studied Al-air battery.

3.4. Molecular simulations

In this section, we first performed a study to explore the morphology of Al crystal. The obtained surface energies (E_{surf}) together with the morphology data for Al crystal are summarized in Table 3. After careful analysis of the obtained data, we can notice that the (111) face accounts for 77.6% of the crystal surface, while 22.4% for (100) face. Our calculated surface energies decrease in the following order: (100) > (111). This is consistent basically with the previous report [33]. Further, a more intuitive micromorphology comparison graph is produced, as depicted in Figure 6. The clean (100) and (111) surfaces possess one type of surface atom with coordination numbers (N for short) 8 and 9, respectively. Consequently, the densely packed Al(111) surface model was chosen as representative to address the adsorption behaviors of the inhibitor because it is the most stable low Miller index Al surface and then the most abundant.

Table 3 Calculated morphology parameters for Al crystal using the BFDH method.

<i>hkl</i>	Multiplicity	d_{hkl}^a (Å)	E_{surf} (J·m ⁻²)	D_{hkl} (Å)	TFA ^b (×10 ³ Å ²)	%TFA ^c	<i>N</i>
(100)	6	2.02	0.95	49.38	7.3	22.4	8
(111)	8	2.33	0.91	42.77	25.3	77.6	9

^a Interplanar distance.

^b The total area of all symmetry images of the facet.

^c The percentage of the total habit surface area occupied by all symmetry images of the facet.

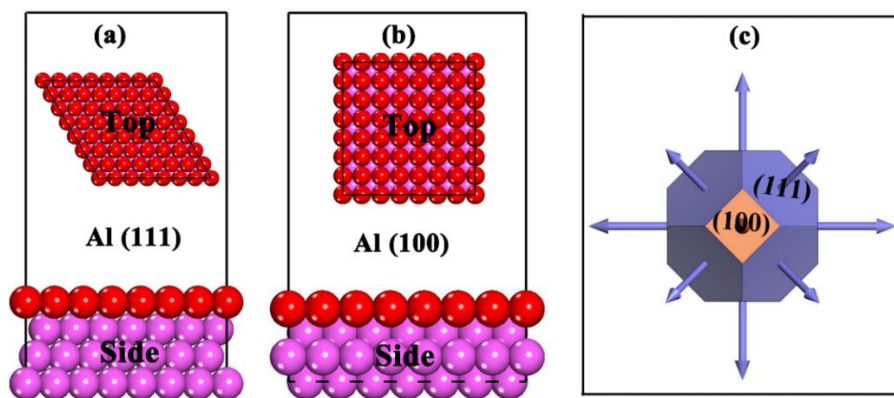


Figure 6. Top and side views of the (a) Al(111) and (b) Al(100) surface models, (c) Wulff plot showing the equilibrium crystal morphology based on the relaxed surface formation energies. Balls in deep red color denote the atoms at the first surface layer.

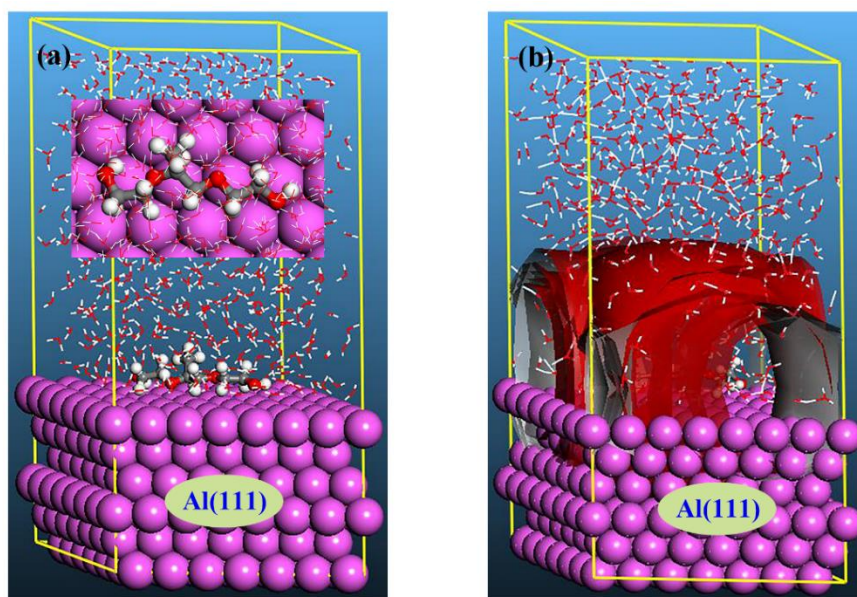


Figure 7. (a) Top and side views of the equilibrium configurations for the PEG-PPG-PEG monomer adsorbed on Al(111) surface; (b) Simulated density field for the inhibitor spread over the metal substrate.

Then, MD simulation was performed in order to get a further insight into the interaction mechanism. The most favorable equilibrium configurations for the PEG-PPG-PEG monomer adsorbed on Al(111) surface is shown in Figure 7a. Obviously, the inhibitor monomer presents a parallel adsorption mode, the molecule is tightly attached on the Al substrate, in order to reach the best surface coverage ability. As depicted in Figure 7b, a strong density field for the polymers can be formed, which prevents the metal surface from getting close to corrosion medium. In addition, for the quantitative evaluation of the adsorption strength, adsorption energy (E_{ads}) was calculated according to the following equation [34, 35]:

$$E_{\text{ads}} = E_{\text{total}} - (E_{\text{surf+water}} + E_{\text{inh+water}}) + E_{\text{water}} \quad (7)$$

where E_{total} is the total potential energy of the system, which includes Al crystal, the adsorbed inhibitor and water molecules; $E_{\text{surf+water}}$ and $E_{\text{inh+water}}$ are the potential energies of the system without the inhibitor and the system without the Al crystal, respectively; E_{water} is the potential energy of the water molecules. The adsorption energies in the present work were calculated from the average adsorption energy of the obtained equilibrium configurations. The obtained E_{ads} value is -249 kJ mol^{-1} . This negative value indicates that spontaneous adsorption can be expected.

3.5. Mechanism of adsorption and inhibition

To further clarify the corrosion inhibition mechanism of PEG-PPG-PEG polymer molecules, an anticorrosion model was proposed, as shown in Figure 8. We can assume that the Al surface is attacked by H_2O molecules and chloride ions in the blank corrosive medium. While in the presence of PEG-PPG-PEG, the inhibitor molecules adsorb on the Al substrate and displace H_2O molecules and chloride ions. The inhibitor film derives from the hybridization interaction between oxygen atoms and the sp -orbitals of the surface Al atoms [36]. Besides, due to the excellent characteristics of PEG-PPG-PEG, i.e., large molecular weight, long molecular chain, and so on, the PEG-PPG-PEG could self-assembly adsorb on the Al surface with weakly chemisorption, which effectively isolates the Al from corrosive medium.

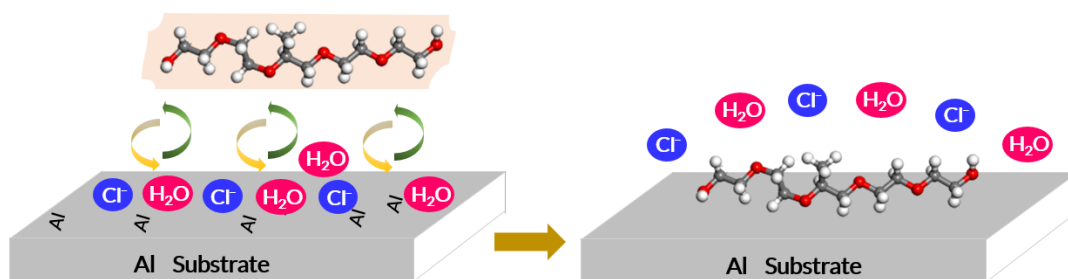


Figure 8. Schematic representation of the inhibition mechanism for PEG-PPG-PEG inhibitor.

4. CONCLUSIONS

The present work aims to explore the effect of PEG-PPG-PEG on the corrosion of Al in Al-air battery electrolyte. Electrochemical and molecular modeling techniques were employed to explore the

inhibition efficiency and mechanism. Our results indicate that the oxygen reduction and corrosion rate of the Al in 3.5% NaCl medium is significantly retarded by adding PEG-PPG-PEG. Its corrosion inhibition efficiency increases with the increasing of concentration and attains a optimal value at 3.0 mM. Tafel test reveals that the PEG-PPG-PEG serves as a mixed-type inhibitor. Theoretical calculations show that anticorrosive film is formed via self-assembly of the polymers on Al surface. Overall, the addition of PEG-PPG-PEG to the battery electrolyte leads to better battery performance. Selecting highly effective additives with appropriate dose is a key research direction for the future development of Al-air batteries.

ACKNOWLEDGEMENTS

This research was sponsored by the National Natural Science Foundation of China (21706195), the Science and Technology Program of Guizhou Province (QKHJC2016-1149), the Guizhou Provincial Department of Education Fundation (QJHKYZ2018-030), the RUDN University Program 5-100, and the Student's Platform for Innovation and Entrepreneurship Training Program (2018521250).

References

1. H. Yadegari and X. Sun, *Acc. Chem. Res.*, 51 (2018) 1532-1540.
2. J.-S. Lee, S. Tai Kim, R. Cao, N.-S. Choi, M. Liu, K. T. Lee and J. Cho, *Adv. Energy Mater.*, 1 (2011) 34-50.
3. Z. H. Meng, H. P. Cai and H. L. Tang, *Int. J. Electrochem. Sci.*, 13 (2018) 5788-5797.
4. M. Mokhtar, M. Z. M. Talib, E. H. Majlan, S. M. Tasirin, W. M. F. W. Ramli, W. R. W. Daud and J. Sahari, *J. Ind. Eng. Chem.*, 32 (2015) 1-20.
5. P. Tan, H. R. Jiang, X. B. Zhu, L. An, C. Y. Jung, M. C. Wu, L. Shi, W. Shyy and T. S. Zhao, *Appl. Energy*, 204 (2017) 780-806.
6. Y. Lai, Q. Wang, M. Wang, J. Li, J. Fang and Z. Zhang, *J. Electroanal. Chem.*, 801 (2017) 72-76.
7. S. S. Sun, H. Miao, Y. J. Xue, Q. Wang, S. H. Li and Z. P. Liu, *Electrochim. Acta*, 214 (2016) 49-55.
8. Y. J. Wu, P. L. Ma, K. Shi, R. N. He, H. Tang, J. P. Zeng, Y. S. Bai, W. Wang and S. Chen, *Int. J. Electrochem. Sci.*, 14 (2019) 4443-4452.
9. D. R. Egan, C. Ponce de León, R. J. K. Wood, R. L. Jones, K. R. Stokes and F. C. Walsh, *J. Power Sources*, 236 (2013) 293-310.
10. I. Smoljko, S. Gudic, N. Kuzmanic and M. Kliskic, *J. Appl. Electrochem.*, 42 (2012) 969-977.
11. J. Ma, J. Wen, J. Gao and Q. Li, *J. Power Sources*, 253 (2014) 419-423.
12. Z. Sun, H. Lu, L. Fan, Q. Hong, J. Leng and C. Chen, *J. Electrochem. Soc.*, 162 (2015) A2116-A2122.
13. M. Pino, D. Herranz, J. Chacón, E. Fatás and P. Ocón, *J. Power Sources*, 326 (2016) 296-302.
14. J. Lee, C. Yim, D. W. Lee and S. S. Park, *Int. J. Pr. Eng. Man-GT.*, 4 (2017) 53-57.
15. M. A. Deyab, *J. Power Sources*, 412 (2019) 520-526.
16. M. A. Deyab, *Electrochim. Acta*, 244 (2017) 178-183.
17. L. T. Popoola, *Corros. Rev.*, 37 (2019) 71-102.
18. K. Khanari, M. Finšgar, M. Knez Hrnčič, U. Maver, Ž. Knez and B. Seiti, *RSC Adv.*, 7 (2017) 27299-27330.
19. C. Schmidt and J. Ulrich, *Chem. Eng. Technol.*, 35 (2012) 1009-1012.
20. L. Guo, W. P. Dong and S. T. Zhang, *RSC Adv.*, 4 (2014) 41956-41967.
21. H. Sun, Z. Jin, C. Yang, R. L. Akkermans, S. H. Robertson, N. A. Spenley, S. Miller and S. M.

- Todd, *J Mol. Model*, 22 (2016) 47.
22. N. A. Al-Mobarak, K. F. Khaled, M. N. H. Hamed, K. M. Abdel-Azim and N. S. Abdelshafi, *Arab. J. Chem.*, 3 (2010) 233-242.
 23. J. Cui, Y. Yang, X. Li, W. Yuan and Y. Pei, *ACS Appl. Mater. Interfaces*, 10 (2018) 4183-4197.
 24. Y. Xu, S. Zhang, W. Li, L. Guo, S. Xu, L. Feng and L. H. Madkour, *Appl. Surf. Sci.*, 459 (2018) 612-620.
 25. L. Guo, S. Zhu and S. Zhang, *J. Ind. Eng. Chem.*, 24 (2015) 174-180.
 26. I. Danaee, O. Ghasemi, G. R. Rashed, M. R. Awei and M. H. Maddahy, *J. Mol. Struct.*, 1035 (2013) 247-259.
 27. S. D. Deng, X. H. Li and H. Fu, *Corros. Sci.*, 53 (2011) 822-828.
 28. F. Y. Cui, L. Guo and S. T. Zhang, *Mater. Corros.*, 65 (2014) 1194-1201.
 29. N. Soltani, H. Salavati, N. Rasouli, M. Pazireh and A. Moghadasi, *Chem. Eng. Commun.*, 203 (2016) 840-854.
 30. V. V. Mehmeti and A. R. Berisha, *Front Chem*, 5 (2017) 61.
 31. D. Sukul, A. Pal, S. K. Saha, S. Satpati, U. Adhikari and P. Banerjee, *Phys. Chem. Chem. Phys.*, 20 (2018) 6562-6574.
 32. S.-m. Li, H.-r. Zhang and J.-h. Liu, *T. Nonferr. Metal. Soc*, 17 (2007) 318-325.
 33. X. Wang, Y. Jia, Q. Yao, F. Wang, J. Ma and X. Hu, *Surf. Sci.*, 551 (2004) 179-188.
 34. Y. El Bakri, L. Guo, E. H. Anouar and E. M. Essassi, *J. Mol. Liq.*, 274 (2019) 759-769.
 35. Y. Qiang, L. Guo, S. Zhang, W. Li, S. Yu and J. Tan, *Scientific Reports*, 6 (2016) 33305.
 36. M. Poberžnik and A. Kokalj, *J. Phys. Chem. C*, 120 (2016) 25915-25922.

© 2019 The Authors. Published by ESG (www.electrochemsci.org). This article is an open access article distributed under the terms and conditions of the Creative Commons Attribution license (<http://creativecommons.org/licenses/by/4.0/>).